

Collaborative fault diagnosis of rotating machinery via dual adversarial guided unsupervised multi-domain adaptation network

Xingkai Chen¹, Haidong Shao^{1*}, Yiming Xiao¹, Shen Yan¹, Baoping Cai², Bin Liu³

1 College of Mechanical and Vehicle Engineering, Hunan University, Changsha 410082, China

2 College of Mechanical and Electronic Engineering, China University of Petroleum, Qingdao 266580 China

3 Department of Management Science, University of Strathclyde, Glasgow G1 1XQ, UK

Corresponding author: Haidong Shao (hdshao@hnu.edu.cn)

Abstract: Most of the existing research on unsupervised cross-domain intelligent fault diagnosis is based on single-source domain adaptation, which fails to simultaneously utilize various source domains with enough and diverse diagnostic information in practical application scenarios. How to better extract common features from multiple domains and integrate multi-source domain knowledge for collaborative diagnosis is a main challenge. To address these problems, a dual adversarial guided unsupervised multi-domain adaptation network (DAG-MDAN) is proposed. Within the proposed framework, the edge adversarial module (EA-Module) in each set of sources-target domain adaptation sub-network is utilized to compute the source-target domain adversarial loss. And an inner adversarial module (IA-Module) is constructed to direct the extraction of common features between multi-source domains, which combined the EA-Module to form the dual adversarial training to enhance domain confusion. Besides, a multi-subnet collaborative decision module (MCD-Module) is designed to compute the confidence scores to assists the multi-subnet classifier to make better fusion decisions. The DAG-MDAN is verified by the several transfer tasks using faulty rotating machinery datasets under the different speed conditions.

Keywords: Rotating machinery fault diagnosis; Dual adversarial training; Multi-subnet collaborative decision making; Transfer learning; Unsupervised multi-domain adaptation

1. Introduction

Rotating machinery plays a significant role in guaranteeing the security of equipment in industrial production [1-8]. Vibration data contains a wealth of information about the operating status of rotating machinery, and intelligent fault diagnosis based on vibration data has received growing attention [9-16]. Deep learning enables to extract deep-level features autonomously for convenient and accurate fault diagnosis in an end-to-end format. However, the intelligent fault diagnosis approach which bases on deep learning requires sufficient labeled samples, and the training samples and test samples are presumed to follow the same distribution [17]. Comparatively, unsupervised cross-domain defect diagnosis, which removes the requirement for a large number of labeled data, is more practicable. [18-25].

The diagnosis of cross-domain mechanical faults has frequently used unsupervised domain adaptation. Qin *et al.* [26] proposed a parameter sharing adversarial domain adaptation network, which constructs a shared classifier to combine domain classifiers and fault classifiers, and the model also included the CORrelation Alignment (CORAL) loss to further increase the domain confusion; Yang *et al.* [27] combined Deep Residual network (ResNet) and polynomial kernel maximum mean discrepancy (PK-MMD) for extracting domain invariant features of faulty bearings; Qian *et al.* [28] designed a domain adaptation network using the convolutional auto-encoder and incorporated CORAL loss with domain classification loss to increase the influence of domain confusion. Li *et al.* [29] added a domain discriminator to the network to perform fault diagnosis for vibration signals at different locations based on adversarial training; Guo *et al.* [30] combined MMD loss and adversarial loss to achieve failure mode recognition of different yet related bearings; Yang *et al.* [31] developed multiple layer adaptation and pseudo label learning regularization term to transfer diagnosis knowledge from lab bearings to loco bearings. The abovementioned unsupervised domain adaptation research studies concentrate on single-source domain adaptation, however, in practical fault diagnosis scenarios, due to large and complex data, selection of a more suitable single source domain often relies on subjective experience. On the other hand, because of the limited information contained, the diagnostic knowledge of a single source domain can hardly cover the target domain. As a

result, multiple source domains with sufficient and diverse diagnostic knowledge are not utilized collaboratively in real scenarios, which reduces the model performance.

In recent years, attentions have paid to the advantages of multi-source domain adaptation methods. In 2020, Li *et al.* [32] designed a multi-classifier network to realize transfer learning from various source domains to the target domain in a weakly supervised scenario; In 2021, Zhu *et al.* [33] transfer diagnostic knowledge from multi-source domains to the target domain using the adversarial learning strategy, and constructed multiple domain discriminators and then assigned weights to multiple domain classification loss; In 2021, Zhang *et al.* [34] constructed multi-source domain classifier in the transfer learning network for fault diagnosis and aligned classifiers by minimizing the discrepancy loss of different classifier results; In 2021, Han *et al.* [35] minimized the triplet loss of multi-source data to improve the intra-class compaction and the inter-class differences at the class level, and the extrinsic domain-level regularization is used by using adversarial training to further lower the danger of overfitting. In 2022, Shen *et al.* [36] applied optimal transport to multi-domain adaptation to form the student–teacher learning, and a cluster optimization is created to help the model make accurate fault diagnosis. In 2022, Li *et al.* [37] designed various multiple kernel maximum mean discrepancies (kMMDs) and combined the reinforcement learning method with domain adaptation method to construct a combination rule for multi-domain-multi-model.

However, shortcomings exist in the existing studies that limit their applicability in fault diagnosis. First, the existing multi-source domain adaptation methods focus on extracting multi-domain features in shared networks, which is difficult to deal with scenarios where the distributions of multi-source domains are significantly different that make it a challenge to extract domain invariant features. In addition, the existing multi domain adaptation methods focus on aligning multiple classifiers, but in fact, they do not sufficiently fuse the multi-source domain features collaboratively, which leads to blindness and instability. Hence, more advanced techniques are demanded to further enhance the accuracy and robustness of unsupervised multi-source domain adaptation for fault diagnosis.

In this paper, a dual adversarial guided unsupervised multi-domain adaptation network is proposed to analyze multi-domain rotating machine vibration data under the different speed working conditions. The comparison results show the superiority and robustness of the DAG-MDAN in unsupervised cross-domain fault diagnosis. The following is a summary of the primary novelties of the proposed DAG-MDAN: 1) Multiple independent source-target domain adaptation sub-networks are constructed to provide sufficient and diverse diagnostic knowledge, and the EA-Module in each sub-network is used to compute the source-target domain adversarial loss. 2) An inner adversarial module is constructed to compute the multi-source domain adversarial loss, which combines multiple edge adversarial module to form dual adversarial training to extract common features between multi-source and target domains and enhances domain confusion. 3) A multi-subnet collaborative decision module is designed to compute the confidence scores using adversarial loss and distribution difference loss of multiple source-target domains, which assists the multi-subnet classifier to make better fusion decisions and reduce the risk of multiple suboptimal decisions while guaranteeing the diversity of decision information.

The remainder of the paper is divided into the following sections. Section 2 introduces multi-domain adaptation problems and details the fundamental theories of maximum mean discrepancy (MMD). Section 3 describes the proposed DAG-MDAN, which includes the source-target domain adaptation subnet with EA-Module, the IA-module, the MCD-Module, and the training process. Section 4 designs two sets of experiments, which prove the proposed approach. Section 5 concludes the article.

2. Preliminary

2.1 Unsupervised multi-domain adaptation problem description

Denote the set with n source domains as $S = \{s_1, s_2, \dots, s_n\}$. The k th source domain s_k contains o_{s_k} samples with labels $X^{s_k} = \{(x_i^{s_k}, y_i^{s_k})\}_{i=1}^{o_{s_k}}$, where $x_i^{s_k} \in R^u$ represents the i th input sample of the k th source domain, and u is the dimensionality of the input sample. $y_i^{s_k} = \{0, 1, \dots, R_{s_k} - 1\}$ represents the collection of R_{s_k} health states for s_k . There are o_T unlabeled samples $X_T = \{x_i^T\}_{i=1}^{o_T}$ in the target domain T . The unsupervised multi-source domain adaptation study aims to construct transfer learning model using the multi-source domains S and target domain T . The following

assumptions are made: 1) a sufficient number of labeled samples exist in each source domain; 2) all unlabeled samples are in the target domain; 3) The sole difference between the source domains and the target domain under different working conditions is in their respective marginal distributions, but the label space and feature space are the same.

2.2 PK-MMD

When comparing two separate but related data sets, the MMD nonparametric distance measure is employed to determine the distribution discrepancy. Given two sets $X = \{x_i | x_i \sim p, i = 1, 2, \dots, \mu\}$, $Y = \{y_j | y_j \sim q, j = 1, 2, \dots, \nu\}$, the MMD is defined as follows [38].

$$D_H := \sup_{\phi \in H} \{E_{x \sim p}[\phi(x)] - E_{y \sim q}[\phi(y)]\} \quad (1)$$

where H stands for the reproducing kernel Hilbert space (RKHS), and $\sup(\cdot)$ represents the input aggregate's supremum. $\phi(\cdot)$ is the mapping function. The MMD between X and Y can be calculated when characteristic kernels are used to make up RKHS as

$$D_H(X, Y) = \frac{1}{\mu^2} \sum_{i=1}^{\mu} \sum_{j=1}^{\mu} k(x_i, y_j) - \frac{2}{\mu\nu} \sum_{i=1}^{\mu} \sum_{j=1}^{\nu} k(x_i, y_j) + \frac{1}{\nu^2} \sum_{i=1}^{\nu} \sum_{j=1}^{\nu} k(x_i, y_j) \quad (2)$$

where $k(\cdot)$ is the characteristic kernels.

In comparison to the conventional Gaussian kernel MMD, a recent study found that PK-MMD has the advantages of low time complexity and parameter robustness [39], which is defined as follows.

$$\mathcal{L}_k^{PK-MMD} = \sum_{k=0}^c \binom{c}{k} a^k b^{c-k} \|E_{x \sim p}(x)_k - E_{y \sim q}(y)_k\|_H^2 \quad (3)$$

$$\|E_{x \sim p}(x)_k - E_{y \sim q}(y)_k\|_H^2 = \frac{1}{\mu\nu} \sum_{i=1}^{\mu} \sum_{j=1}^{\nu} [k(\mathcal{F}_i^{s_k}, \mathcal{F}_j^{s_k}) - 2k(\mathcal{F}_i^{s_k}, \mathcal{F}_j^{t_k}) + k(\mathcal{F}_i^{t_k}, \mathcal{F}_j^{t_k})] \quad (4)$$

$$k(x, y) = (ax^T y + b)^c \quad (5)$$

in which a, b, c represent the slope, intercept and order of the polynomial kernel, respectively.

The purpose of adding PK-MMD is to assist the model in reducing the difference in the distribution of the source and target domains and as an evaluation criterion for the MCD-Module confidence scores.

3. Proposed method

The architecture of the developed DAG-MDAN can be seen in **Fig. 1**, which includes of multiple independent source-target domain adaptation sub-networks, an inner adversarial module and a multi-subnet collaborative decision module. A CNN feature extractor, an EA-Module, and a classifier make up each subnet. The EA-Module is responsible for one specific domain classification task and giving the adversarial loss, and the classifier gives the classification result of the current subnet and the classification loss. The inner adversarial module receives the source domain features extracted from each subnet, identifies these features from the source domain to which they belong, and gives the inner adversarial loss. The multi-subnet collaborative decision module receives and fuses the predicted probabilities of each subnet classifier, and gives the final collaborative diagnosis results.

3.1 Source-target domain adaptation sub-networks

Domain-invariant features are independently extracted using several sets of source-target domain adaptation sub-networks. **Fig. 2** depicts the precise structure of each subnet, which consists of three domain adversarial layers (Adv1-Adv3), two fully connected layers (F1, F2), and four convolutional layers (Conv1-Conv4). The specific parameters are shown in **Table 1**. Given the k th set of source-target domain samples $\{(x_i^{s_k}, x_i^{t_k}) | i = 1, 2, \dots, m\}$ in the input layer, where m represents the number of samples contained in each batch, the source-target sample are converted into high-level transferrable features by four convolutional layers. To lower the dimensionality of learning features, the MaxPool is included in the second convolutional layer, and the AdaptiveMaxPool is subsequently adopted in the fourth convolutional layer. The ReLU activation function is used to prevent the gradient vanishing or explosion issue. All

convolutional layers are subjected to batch normalization (BN) in order to reduce the danger of over-fitting and speed up the training process. After passing through the F1 layer the high-level features will be flattened as the one-dimensional input vector of the classifier. Assume $F_k(\cdot)$ represents the feature extractor of the k th sub-networks, then the feature $\mathcal{F}_i^{D_k} = (\mathcal{F}_i^{s_k}, \mathcal{F}_i^T)$ can be expressed as

$$\mathcal{F}_i^{D_k} = F_k(x_i^{D_k}, \theta^{D_k, F}) \quad (6)$$

where $x_i^{D_k} = (x_i^{s_k}, x_i^T)$ is the input samples of the k th sub-networks, and $\theta^{D_k, F}$ denotes the training parameters of the feature extractor.

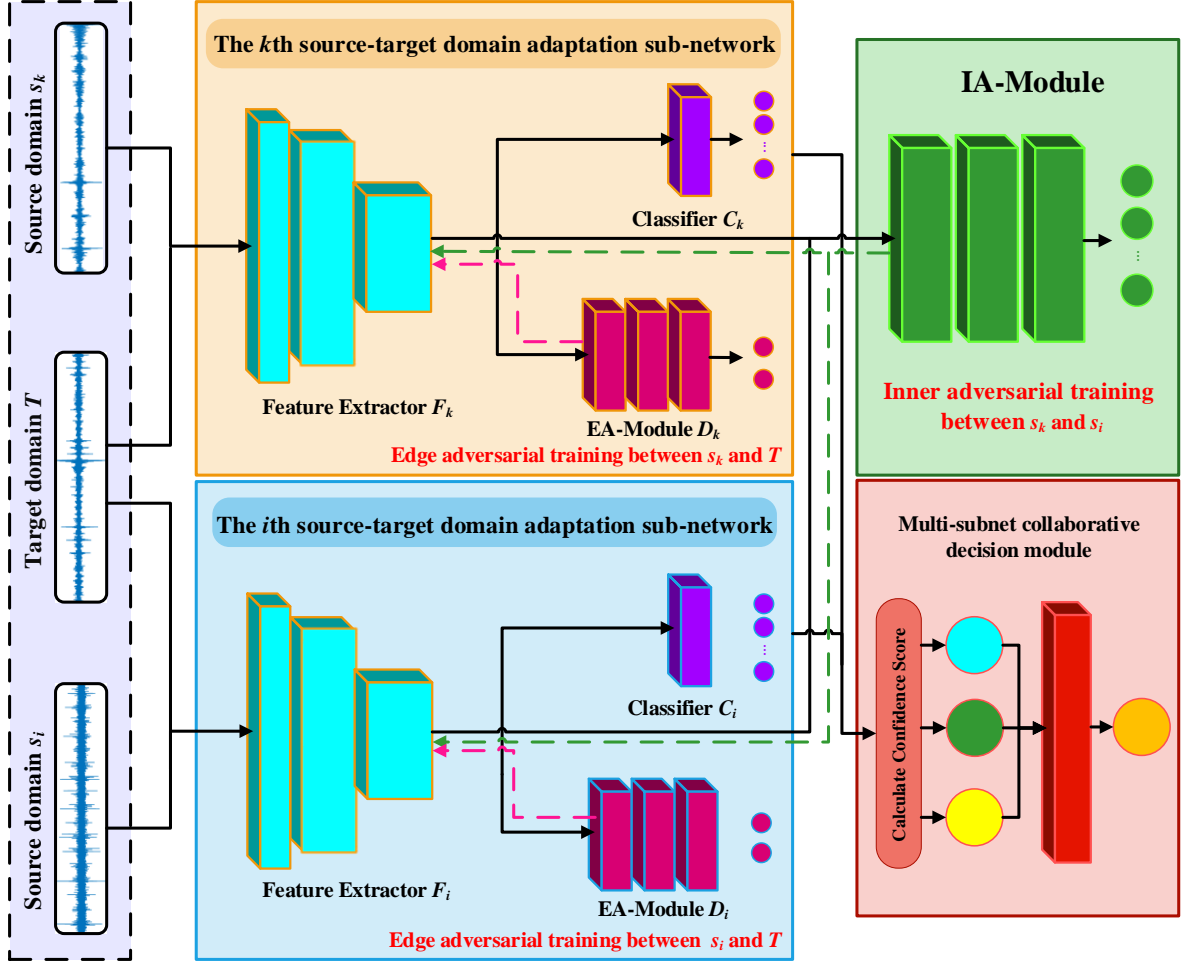


Fig. 1. The architecture of DAG-MDAN for the task $(s_i, s_k) \rightarrow T$.

The Softmax function is used by F2 layer to predict the probability of each sample being related to the health states, which can be expressed as

$$P_k^{D_k} = C_k^{\text{Softmax}}(\omega^{D_k} \mathcal{F}_i^{D_k} + b^{D_k}) \quad (7)$$

where $C_k^{\text{Softmax}}(\cdot)$ is the classifier for the k th sub-networks, $\theta^{D_k, C} = (\omega^{D_k}, b^{D_k})$ is the training parameters of the classifier $C_k^{\text{Softmax}}(\cdot)$. By back-propagating the classification loss, which is also known as the cross-entropy loss, and can be calculated as follows.

$$\mathcal{L}_k^c = -\frac{\alpha^{s_k}}{m} \sum_{i=1}^m \sum_{j=0}^{R_{s_k}-1} I[y_i^{s_k} = j] \log[C_k^{\text{Softmax}}(\mathcal{F}_i^{s_k})] \quad (8)$$

where $I(\cdot)$ is the indicator function, $C_k^{\text{softmax}}(\mathcal{F}_i^{s_k})$ indicates the predicted probability of the k th source domain sample feature $\mathcal{F}_i^{s_k}$ belonging to the k th class of health states, α^{s_k} is the penalty factor.

The feature extractor F_k cooperates the EA-Module D_k to extract domain common features via an adversarial training process [40]. The EA-Module is responsible for discriminating the source and target domains of each subnet. The domain discriminator layers Adv1 and Adv2 use the Leaky-ReLU activation function and Adv3 uses the Sigmoid activation function; Adv1~Adv3 layers are all fully connected layers. The domain adversarial loss is defined as the binary cross-entropy loss, which can be expressed as

$$\mathcal{L}_k^d = -\alpha_k^{\text{adv}} \left\{ \frac{1}{o_{s_k}} \sum_{i=1}^{o_{s_k}} \log[D_k(\mathcal{F}_i^{s_k})] + \frac{1}{o_T} \sum_{i=1}^{o_T} \log[(1 - D_k(\mathcal{F}_i^T))] \right\} \quad (9)$$

where $D_k(\mathcal{F}_i^{s_k})$ and $D_k(\mathcal{F}_i^T)$ denote the predicted probability of the k th pair of source-target domains i th sample belonging to the source or target domain, α_k^{adv} is the penalty factor.

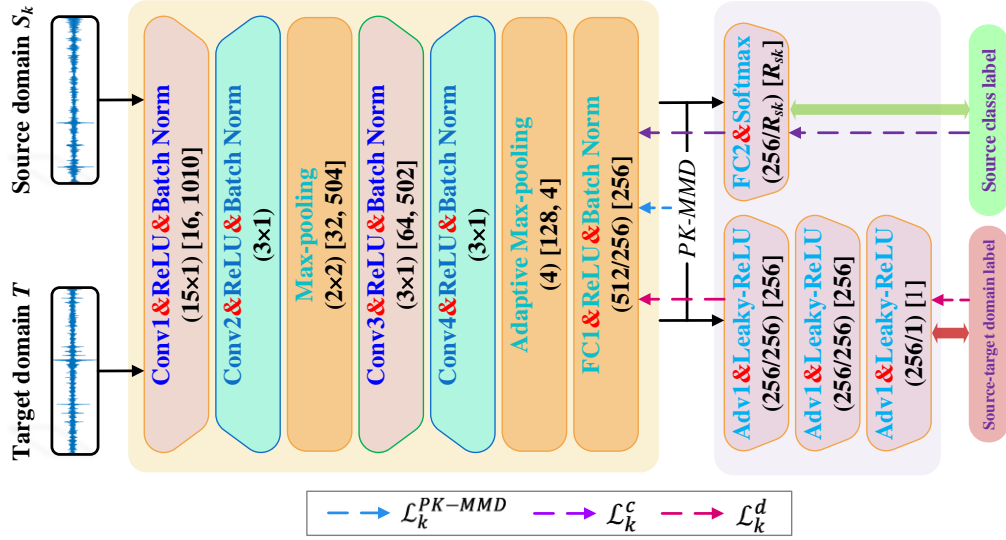


Fig. 2. The architecture of the source-target domain adaptation sub-networks for s_k and T .

Table 1

The structure hyperparameter settings of the developed source-target domain adaptation sub-networks.

Layers	Parameter sizes	Activation functions	Output sizes
Input	/	/	1×1024
Conv1	Kernel 15, Stride 1; BN	ReLU	16×1010
Conv2	Kernel 3; Stride 1; BN; MaxPool: 2×2	ReLU	32×504
Conv3	Kernel 3, Stride 1; BN	ReLU	64×502
Conv4	Kernel 3, Stride 1; BN; AdaptiveMaxPool: 4	ReLU	128×4
F1	512/256; BN	ReLU	256
F2	256/ R_{s_k}	Softmax	R_{s_k}
Adv1	256/256	Leaky-ReLU	256
Adv2	256/256	Leaky-ReLU	256
Adv3	256/1	Sigmoid	1

3.2 Inner adversarial module

An inner adversarial module is constructed by adding an additional domain discriminator D_i for multi-subnet source domain features, which serves to discriminate the domains that contain multi-source domain features. The IA-Module combined EA-Module aids to extract domain invariant features between multi-source and target domains, which better transfers fault diagnosis knowledge from multi-source domain to the target domain. The parameters of IA-Module are shown in Table 2. The IA-Module collects the features $\mathcal{F}_i^S = \{(\mathcal{F}_i^{s_1}, \mathcal{F}_i^{s_2}, \dots, \mathcal{F}_i^{s_k}) \mid k = 1, 2, \dots, n\}$ from multi-source domains, where

$$\mathcal{F}_i^{s_k} = F_k(x_i^{s_k}, \theta^{\mathcal{D}_k^F}) \quad (10)$$

Inner adversarial loss \mathcal{L}^{IA} is defined as cross-entropy loss, calculated as follows.

$$\mathcal{L}^{IA} = \frac{1}{m} \sum_{i=1}^m \sum_{j=1}^n I\{Y_i^S = j\} \log[D_I(\mathcal{F}_i^S)] \quad (11)$$

where $Y_i^S = \{1, 2, \dots, n\}$ represents domain label of multi-source domains, and $D_I(\mathcal{F}_i^S)$ given by the IA-Module is the predicted probability of the current sample belonging to the j th source domain.

The source-target domain subnet with EA-Module extracts invariant features between certain source domain and target domain (**Fig. 3(a)**), and the IA-Module fuses multi-source domain features by dual adversarial loss (as in **Fig. 3(b)**). Both the IA-Module and source-target domain adaptation subnet jointly extract invariant features from multi-source domains, so that the diagnostic knowledge can better cover the target domain.

Table 2

The structure hyperparameter settings of the developed IA-Module.

Layers	Parameter sizes	Activation functions	Output sizes
IAdv1	256/256	Leaky-ReLU	256
IAdv2	256/256	Leaky-ReLU	256
IAdv3	256/3	/	3

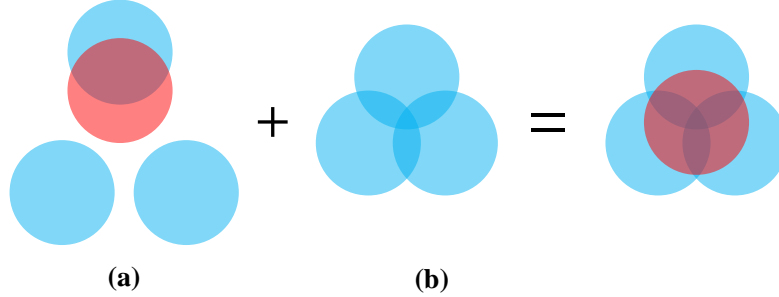


Fig. 3. IA-Module combines EA-Module to form dual adversarial training to learn multi-domain invariant features.

3.3 Multi-subnet collaborative decision module

When receiving the same target domain samples and diagnosing their health status separately, multi-subnet may make different decisions. The existing strategies mostly focus on aligning multiple classifiers, which, however, fails to sufficiently utilize the multi-source domain diagnostic information. A multi-subnet collaborative decision module is designed, which uses the adversarial loss and discrepancy loss of each sub-net as the evaluation index and calculates the confidence score. The confidence score is used to analyze and compare the feature fitting capability of multi-subnet and finally realize the collaborative decision of multi-domain diagnostic information. The decision process can be expressed as:

$$y_i^T = \begin{cases} \arg \max(P_k^t) & \text{if } \arg \max(P_1^t) = \arg \max(P_2^t) = \dots = \arg \max(P_k^t) \\ \max(\text{Score}_k) & \text{else } \arg \max(P_1^t) \neq \arg \max(P_2^t) \end{cases} \quad (12)$$

$$\text{Score}_k = -\tau_k^{sc} \frac{\mathcal{L}_k^{\text{PK-MMD}}}{\sum_{k=1}^n \mathcal{L}_k^{\text{PK-MMD}}} + (1 - \tau_k^{sc}) \frac{\mathcal{L}_k^d}{\sum_{k=1}^n \mathcal{L}_k^d} \quad (13)$$

$$P_k^t = C_k^{\text{softmax}}(\omega^{\mathcal{D}_k} \mathcal{F}_i^t + b^{\mathcal{D}_k}) \quad (14)$$

where the confidence score $\text{Score} = \{\text{Score}_1, \text{Score}_2, \dots, \text{Score}_k \mid k = 1, 2, \dots, n\}$, P_k^t is the predicted probability of the target domain samples given by the k th source-target domain adaptation subnet-work classifier, and $\tau_k^{sc} \in (0, 1)$ is the preconditioning factor, which was set to 0.5 in this article. **Fig. 4** shows the schematic diagram of the multi-subnet collaborative decision module.

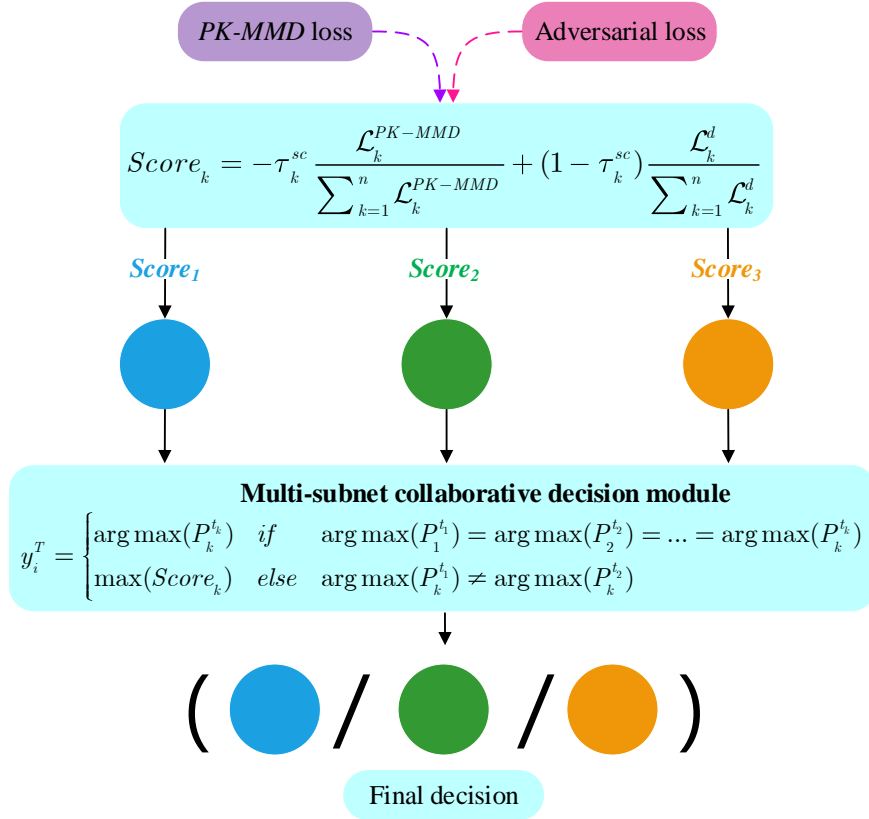


Fig. 4. The algorithm of MCD-Module.

3.4 Training process

Three steps are involved in DAG-MDAN training. Firstly, the feature extractor and classifier in the source-target domain adaptation sub-networks are trained through the data with labels from input source samples, and the optimization objectives are as follows.

$$\max_{\{\theta^{D_k,F}, \theta^{D_k,C} | k \in (1,2,\dots,n)\}} \sum_{k \in (1,2,\dots,n)} \mathcal{L}_k^c \quad (15)$$

The sample from the source-target domains are then jointly used to train the model. While minimizing the PK-MMD loss optimized feature extractors to reduce the distribution discrepancy in the source-target domain, several EA-Modules are optimized to learn the domain-invariant features in the source-target domain based on the various distribution baselines of different source-domain samples, and with following optimization objectives:

$$\max_{\{\theta^{D_k,D} | k \in (1,2,\dots,n)\}} \sum_{k \in (1,2,\dots,n)} \mathcal{L}_k^d \quad (16)$$

$$\max_{\{\theta^{D_k,F} | k \in (1,2,\dots,n)\}} \sum_{k \in (1,2,\dots,n)} \mathcal{L}_k^{PK-MMD} \quad (17)$$

where $\theta^{D_k,D}$ is the training parameters of the EA-Module.

Finally, the dual adversarial loss \mathcal{L}^A is used to update the IA-module and optimize the feature extractor of each subnet.

$$\max_{\{\theta^{D_k,D_e}\}} \mathcal{L}^A \quad (18)$$

The total optimization problem can be stated as follows using stochastic gradient descent (SGD):

$$\begin{aligned} \theta^{D_k,F} &\leftarrow \{\theta^{D_k,F} - \rho(\mathcal{L}_k^c + \mathcal{L}_k^{PK-MMD} - \mathcal{L}^A) | k \in (1,2,\dots,n)\} \\ \theta^{D_k,C} &\leftarrow \{\theta^{D_k,C} - \rho\mathcal{L}_k^c | k \in (1,2,\dots,n)\} \\ \theta^{D_k,D} &\leftarrow \{\theta^{D_k,D} - \rho\mathcal{L}_k^d | k \in (1,2,\dots,n)\} \end{aligned} \quad (19)$$

where ρ is the learning rate.

4. Case studies

4.1 Comparison experiments and implementation detail

Given two unsupervised multi-domain rotating machinery fault diagnosis cases to verify the advantage of the proposed method, the DAG-MDAN is compared with several different mainstream methods:

- 1) CNN without domain adaptation (CNN): This method consists of a feature extractor and a classifier and only considers the classification loss of the source domain samples, which is adopted the baseline for the experiment.
- 2) PK-MMD-based domain adaptation method (PK-MMD): The network structure in this method consists of a feature extractor, a classifier and the MMD adaptation layer to optimize the training parameters by minimizing PK-MMD loss and classification loss.
- 3) Single source domain based DANN (S-DANN): In this method, a feature extractor, a classifier, and a domain discriminator make up the network structure. Since k source domains exist, k models will be produced. We choose the option that performs the best in terms of classification accuracy on the test dataset.
- 4) Multiple source domain based DANN (M-DANN): This approach is an expansion of the comparison method 3), combining three source domains as input and sharing a feature extractor, a classifier and a domain discriminator to optimize the network parameters by back-propagating the classification loss and adversarial loss.
- 5) Multiple source domain adaptation with classifier alignment (ADACL): This method consists of a feature extractor, a domain discriminator and multiple classifiers, and achieves multi-source domain migration by aligning the outputs of different classifiers and optimizing the network parameters by back-propagating classification loss, adversarial loss, and classifier alignment loss.

The hyperparameters of the feature extractors, classifiers, and domain discriminators included in all compared methods are consistent with the proposed methods. Ten replicate experiments were performed for each method to reduce the effect of randomness. The relevant parameters' specifics are as follows: The network structure is trained using the SGD optimizer and has a momentum of 0.85. The number of batch samples is 32, and the initial learning rate is 0.1. The learning rate falls to 20% of the initial rate after 100 iterations, and the total loss is compounded by a penalty factor that ranges from 0 to 1 to suppress noisy signals in the early stages of training. This penalty factor can be calculated as follows:

$$\rho = \frac{2}{1 + \exp(-\gamma(\frac{e}{E}))} - 1 \quad (20)$$

e indicates e th epoch in the training, E indicates the number of the epoch, and γ is 10. The proposed DAG-N is performed on the computation platform: GPU NVIDIA GTX 1650, CUDA 10.0, and Pytorch 1.7.1.

4.2 Case I: unsupervised multi-domain adaptation bearing fault diagnosis

4.2.1 Bearing datasets descriptions

As shown in **Fig. 5** [41], the analyzed bearing data is gathered from roller bearings operating in a laboratory under conditions of speed fluctuation at a sample frequency of 25.6 kHz. The platform can mimic the bearing in four different health states, including normal (N), inner fault (IF), outer fault (OF), and rolling fault (RF), which are denoted, respectively, by labels 0, 1, 2, and 3, with three kinds of health states. Bearing data under four operating conditions (900 r/min , 1200 r/min , 1500 r/min and variable speed, respectively) were selected to construct three source domains and target domain. More details are shown in **Table 3**.

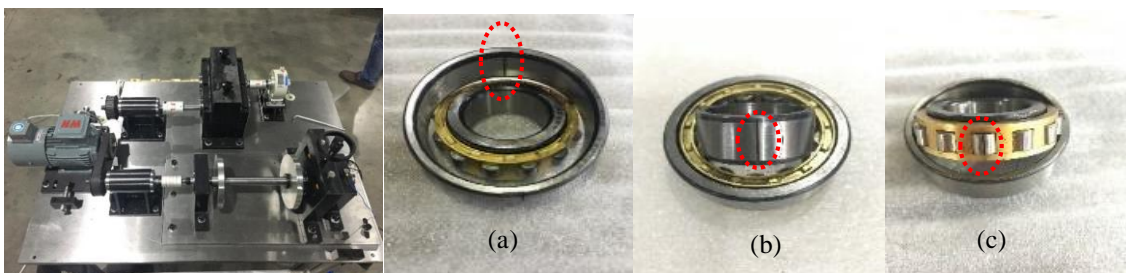


Fig. 5. Pictures of the QPZZ-II test-rig and the fault bearings (a) OF; (b) IF; (c) RF.

Table 3

Introduction to the bearing fault diagnosis transfer tasks.

Tasks	The working conditions		Number of samples			Fault categories
	Source domain (r/min)	Target domain (r/min)	Source training	Target training	Target testing	
$R_1, R_2, R_3 \rightarrow R_4$	900, 1200, 1500	Time-varying speeds	678×3	678	170	Four conditions (labels 0-3)
$R_1, R_2, R_4 \rightarrow R_3$	900, 1200, Time-varying speeds	1500	678×3	678	170	
$R_1, R_3, R_4 \rightarrow R_2$	900, 1500, Time-varying speeds	1200	678×3	678	170	
$R_2, R_3, R_4 \rightarrow R_1$	1200, 1500, Time-varying speeds	900	678×3	678	170	

Note: Time-varying means that the speed varies from 900 to 1500 r/min .

4.2.2 Analysis of experiment results in Case I

The experimental results are listed in **Table 4**, and the average accuracy of ten experiments was used as the experimental results. Since the transfer task $R_2, R_3, R_4 \rightarrow R_1$ have the lowest diagnostic accuracy among the four transfer tasks, which was selected to show the iterations of each method as shown in **Fig. 7**. **Fig. 8** shows the fluctuation of the DAG-MDAN and each comparison method for ten experiments in four tasks; **Fig. 6** shows the ring diagram created to more visually represent the accuracy of each method.

The following inferences can be made from the aforementioned graphs and figures:

- 1) By comparing the DAG-MDAN with other methods in **Table 4** and **Fig. 6**, it is evident that the DAG-MDAN has the highest diagnostic accuracy rate of all diagnostic approaches, with an average fault diagnosis accuracy rate of 97.65%; **Fig. 8** shows that the DAG-MDAN fluctuates more smoothly than other approaches, which indicates its robustness.
- 2) By comparing the results of CNN without domain adaptation module and methods with domain adaptation module in different tasks, it is clear that the performance of CNN is poor, which indicates that CNN without domain adaptation module are difficult to finish transfer diagnosis tasks well once the target domain feature distribution is complex. In this case the method with domain adaptation module can help the model to improve the diagnostic accuracy. However, we noticed that the CNN and MMD converge faster and the accuracy rate floats smoothly, which indicates that CNN and MMD have a more lightweight and stable structure, which is beneficial to the rapid convergence of the model.
- 3) By comparing S-DANN and M-DANN, it is observed that in most cases the multi-source domain adaptation method has better performance. But through the transfer task $R_1, R_2, R_4 \rightarrow R_3$, it is noted that in some scenarios just combining the source domain data may lead to negative transfer, which also illustrates the necessity for reasonable fusion of multiple source domain data.
- 4) **Fig. 7** shows that the DAG-MDAN has the ability to break the bottleneck in the training process compared with other methods, and the DAG-MDAN still achieves more than 90% diagnostic accuracy even when other methods perform poorly.

Table 4

Fault diagnosis accuracy on multi-domain bearing fault diagnosis transfer tasks-

Methods	Unsupervised multi-domain bearing fault diagnosis transfer tasks				Average
	$R_1, R_2, R_3 \rightarrow R_4$	$R_1, R_2, R_4 \rightarrow R_3$	$R_1, R_3, R_4 \rightarrow R_2$	$R_2, R_3, R_4 \rightarrow R_1$	
CNN	77.75±1.90%	86.25±1.52%	79.37±1.79%	70.63±1.95%	78.50%
PK-MMD	90.87±1.16%	95.44±0.84%	92.37±1.00%	82.49±2.74%	90.30%
S-DANN	92.31±2.09%	98.13±1.01%	93.43±1.26%	85.38±3.19%	92.31%
M-DANN	94.31±0.44%	94.50±1.65%	95.75±1.08%	88.81±1.59%	93.34%
ADACL	93.94±0.49%	99.50±0.61%	96.90±0.72%	89.62±2.11%	94.99%
DAG-MDAN	98.19±0.52%	99.80±0.28%	99.00±0.42%	93.63±0.54%	97.65%

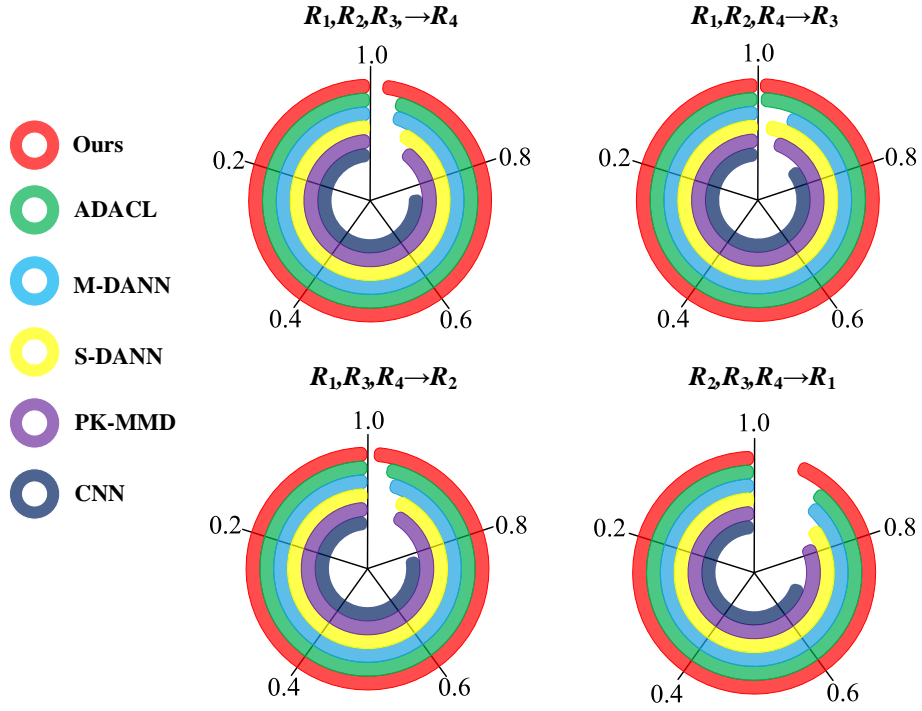


Fig. 6. Accuracy rings for each method in different bearing fault diagnosis transfer tasks.

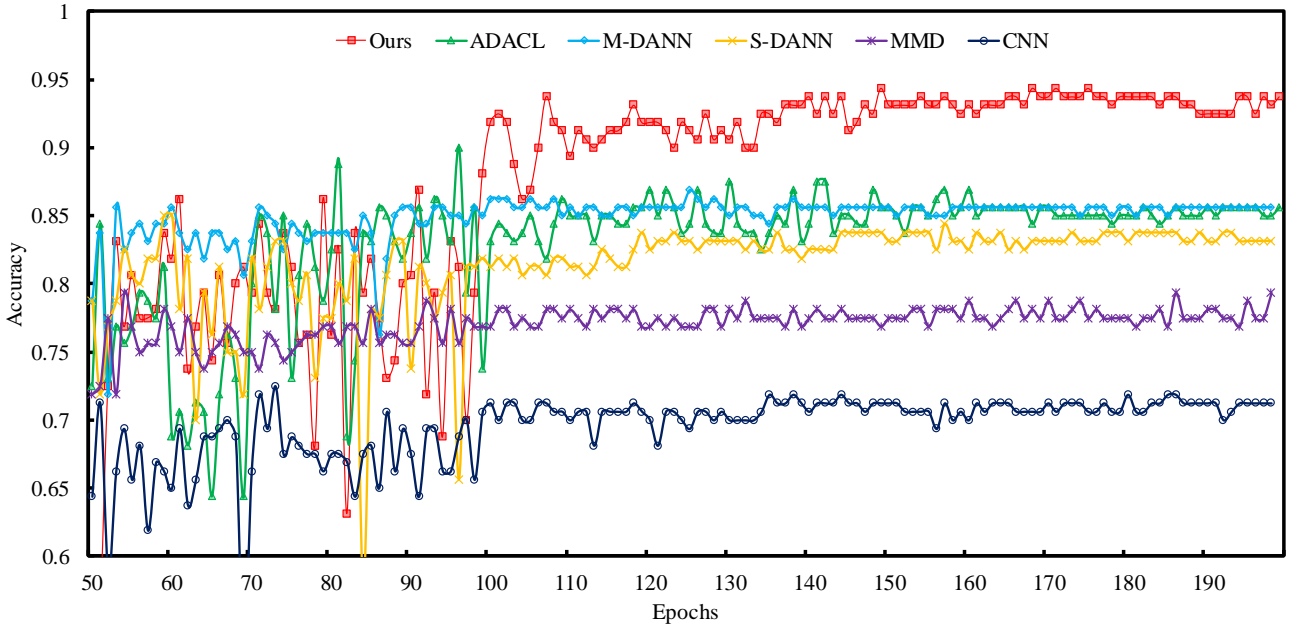


Fig. 7. Convergence of each method in the bearing fault diagnosis transfer task $R_2, R_3, R_4 \rightarrow R_1$.

4.2.3 Effectiveness of dual adversarial training

To give more effective analysis of the dual adversarial training, this section is designed for the high-level feature visualization by having two methods with or without IA-Module through the t-distributed stochastic neighbor embedding (t-SNE) technique [42]. The advantages of the dual adversarial training are verified by comparing the feature distributions of the two methods. $R_1, R_2, R_3 \rightarrow R_4$ is chosen as the scenario to highlight the advantages of the internal adversarial module due to the high migration difficulty and poor performance of the methods in the $R_1, R_2, R_3 \rightarrow R_4$ task, as well as the complex fault characteristics in the target domain with variable speed conditions.

Fig. 9 shows the features extracted from each bearing health state in task $R_1, R_2, R_3 \rightarrow R_4$ by both methods, which can be found by comparison: The dual adversarial training has a significantly positive effect on the model to effectively fuse diagnostic knowledge from multiple source domains and cover the target domain. By comparing (a), (b), (c), (d)

and (e), (f), (g), (h), it can be found that after removing the IA-Module, the target domain will only overlap with at most one source domain, which will lead to lack of diagnosis information and the source domain is not easy to cover the target domain comprehensively; After the optimization by the dual adversarial training, (c), (d) show that the features of the three source and target domains are fused (Figure (c) is scaled to enlarge the display), and (a), (b) show that the dual adversarial training effectively uses at least two of the three source domains for the target domain diagnosis. The rationality and practicality of the DAG-MDAN in the field of unsupervised cross-domain fault diagnosis is demonstrated by an intuitive analysis of the feature distribution.

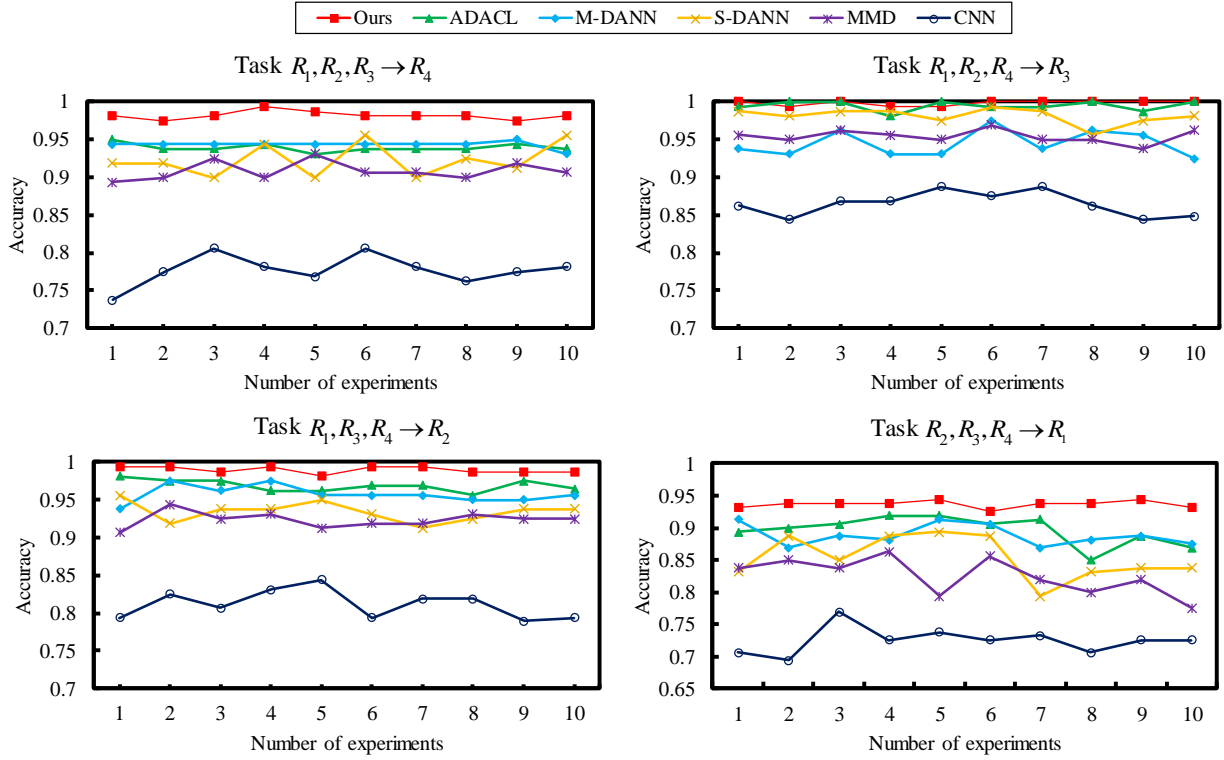


Fig. 8. Accuracy of 10 experiments with different methods in each bearing fault diagnosis transfer task.

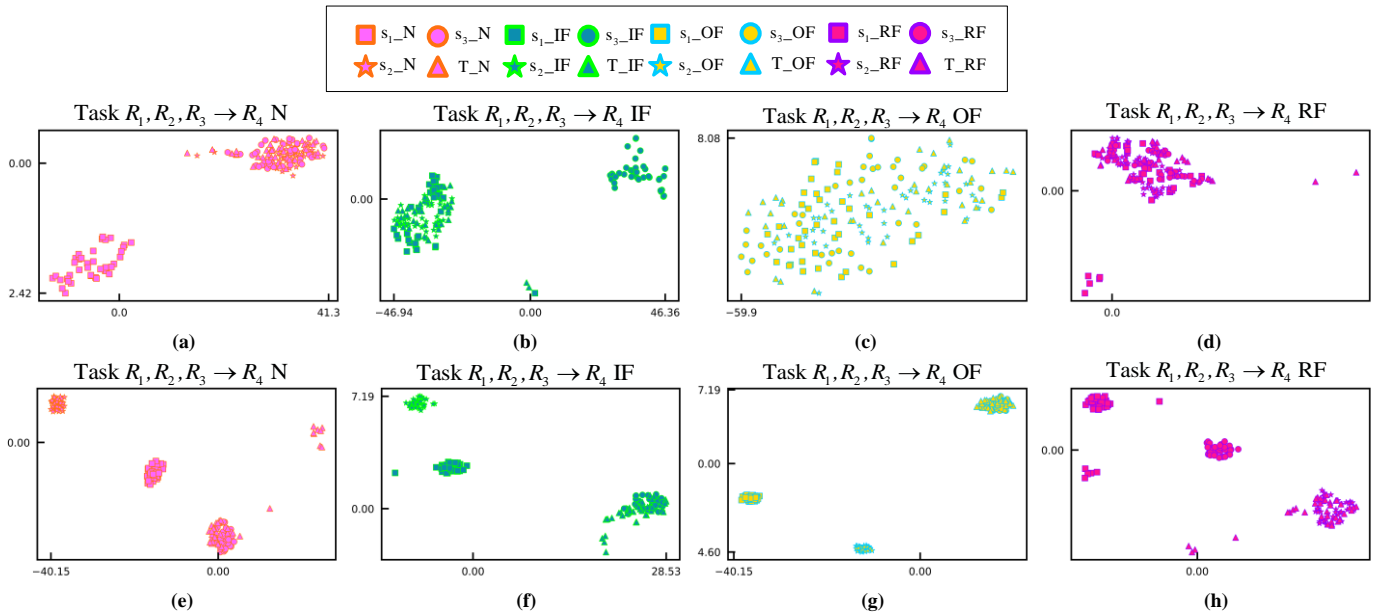


Fig. 9. Feature distribution under the bearing fault diagnosis transfer task $R_1, R_2, R_3 \rightarrow R_4$: (a)(b)(c)(d) With IA-Module; (e)(f)(g)(h) Without IA-Module

4.2.4 Advantages of multi-subnet collaborative decision module

To further show the advantages of the proposed MCD-Module, a comparison test with and without the multi-subnet collaborative decision module is set up. The network structure of the without MCD-Module is consistent with the proposed method, and the average of the multi-classifier outputs is used as the final output. Experiments were conducted in four transfer fault diagnosis tasks, and the experimental results are shown in **Fig. 10**. Since this paper uses an algorithm in which the learning rate decreases with epoch when training the model, the initial learning rate is larger during the training process to find a suitable global optimal solution; in the later stage of training, the learning rate is smaller to find a local optimal solution. Therefore, it causes the phenomenon that the accuracy rate fluctuates greatly in the early training period and is smoother in the later training period. As can be observed from the comparison experiments (1) in the early stage of training process without convergence, the model embedded multi-subnet collaborative decision module has less variation in diagnostic accuracy than the model removed multi-subnet collaborative decision module; (2) in the late stage of training process with convergence, the model embedded multi-subnet collaborative decision module has higher diagnostic accuracy than the model removed multi-subnet collaborative decision module. It indicates that the multi-subnet collaborative decision module can not only make better decisions when the model performance is poor by reasonably using the multi-source domain knowledge, but also help the model to further improve the diagnostic accuracy in the later stage of training process.

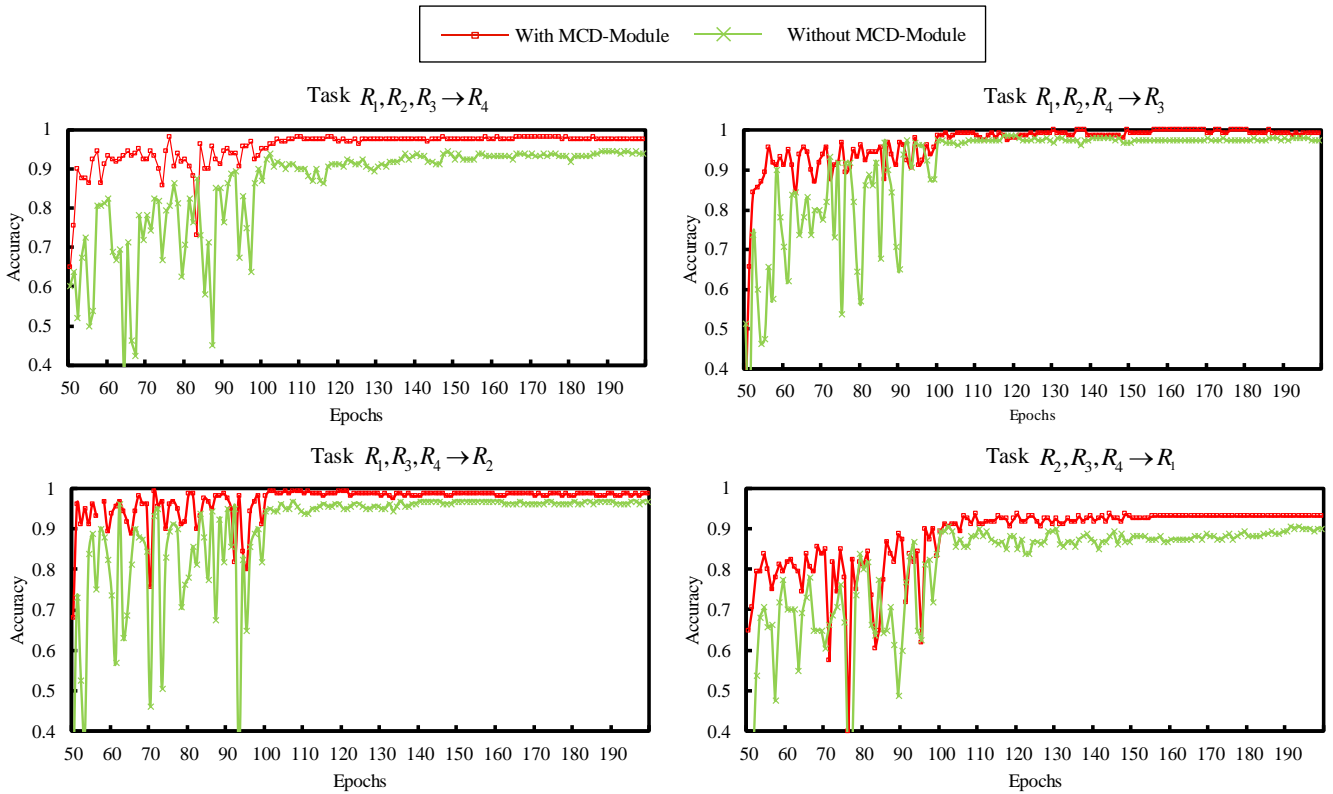


Fig. 10. Accuracy comparison between the training process of with MCD-Module and without MCD-Module

4.3 Case II: analysis of the gearbox datasets

4.3.1 Datasets Descriptions: gearbox datasets

The Prognostics and Health Management 2009 Challenge data are used to create the gearbox dataset. **Fig. 11** shows the interior of the gearbox, which includes six bearings (three on output side: OS and three on input side: IS), three axes (input axis (IS), intermediate axis (ID), output axis (OS)) and four gears. This dataset considers eight health states (labels 0-7). In this article four rotating speeds are used to construct four unsupervised multi-domain gearbox transfer tasks, namely 30 Hz (R_5), 35 Hz (R_6), 40 Hz (R_7) and 45 Hz (R_8). 66.7 kHz is used as the sample frequency. Tables 5 and 6 provide more information.

Table 5

Label description of the gearbox.

Labels	Gear				Bearing				Shaft			
	32T	96T	48T	80T	IS:IS	ID:IS	OS:IS	IS:OS	ID:OS	OS:OS	Input	Output
0	Good	Good	Good	Good	Good	Good	Good	Good	Good	Good	Good	Good
1	Chipped	Good	Eccentric	Good	Good	Good	Good	Good	Good	Good	Good	Good
2	Good	Good	Eccentric	Good	Good	Good	Good	Good	Good	Good	Good	Good
3	Good	Good	Eccentric	Broken	Ball	Good	Good	Good	Good	Good	Good	Good
4	Chipped	Good	Eccentric	Broken	Inner	Ball	Outer	Good	Good	Good	Good	Good
5	Good	Good	Good	Broken	Inner	Ball	Outer	Good	Good	Good	Im	Good
6	Good	Good	Good	Good	Inner	Good	Good	Good	Good	Good	Good	Ks
7	Good	Good	Good	Good	Good	Ball	Outer	Good	Good	Good	Im	Good

Note: Im: imbalance; Ks: keyway sheared.

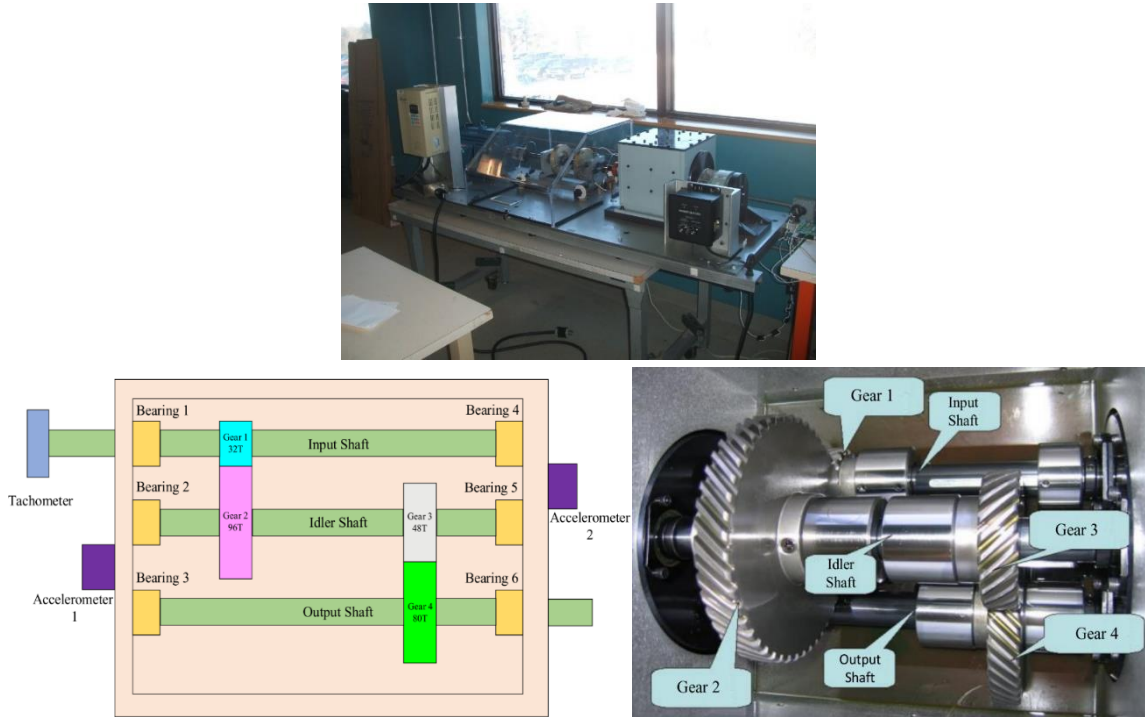

Fig. 11. Pictures of gearbox and the inside detail.

Table 6

Introduction to the gearbox fault diagnosis transfer tasks.

Tasks	The working conditions		Number of samples			Fault categories
	Source domains (Hz)	Target domain (Hz)	Source training	Target training	Target testing	
$R_5, R_6, R_7 \rightarrow R_8$	30, 35, 40	45	640×3	640	160	Eight conditions (labels 0-7)
$R_5, R_6, R_8 \rightarrow R_7$	30, 35, 45	40	640×3	640	160	
$R_5, R_7, R_8 \rightarrow R_6$	30, 40, 45	35	640×3	640	160	
$R_6, R_7, R_8 \rightarrow R_5$	35, 40, 45	30	640×3	640	160	

4.3.2 Analysis of experiment results in Case II

In this subsection, the same comparison experiments and parameter settings are set up as in **Case I**, and the experiment with (without) the IA-Module and with (without) MCD-Module are also preformed. The accuracy of the proposed method and the comparison method for different transfer tasks are shown in the **Table 7** and **Fig. 13**. Since the transfer task $R_6, R_7, R_8 \rightarrow R_5$ have the lowest diagnostic accuracy among the four transfer tasks, which was selected to show the iterations of each method as shown in **Fig. 12**. **Fig. 14** shows the fluctuation of the DAG-MDAN and each

comparison method for ten experiments in different transfer tasks; **Fig. 15** and **Fig. 16** show the effectiveness of the dual adversarial module and the multi-subnet collaborative decision module, respectively. Same instructions as **Case I**.

Table 7

Fault diagnosis accuracy on the multi-domain gearbox fault diagnosis transfer tasks.

Methods	Unsupervised multi-domain gearbox fault diagnosis transfer tasks				Average
	$R_5, R_6, R_7 \rightarrow R_8$	$R_5, R_6, R_8 \rightarrow R_7$	$R_5, R_7, R_8 \rightarrow R_6$	$R_6, R_7, R_8 \rightarrow R_5$	
CNN	66.19±4.14%	71.44±3.98%	67.75±3.73%	61.63±3.95%	66.75%
PK-MMD	71.94±3.94%	85.06±2.31%	79.06±2.73%	75.31±1.70%	77.84%
S-DANN	79.63±3.18%	89.81±1.31%	86.25±2.03%	78.62±2.16%	83.58%
M-DANN	84.50±2.16%	90.25±1.84%	81.75±2.22%	83.44±2.22%	84.99%
ADACL	86.94±3.25%	90.75±1.39%	88.37±2.28%	85.88±3.37%	87.99%
DAG-MDAN	94.00±2.36%	94.94±2.12%	94.44±0.95%	91.86±1.28%	93.81%

From the above figures and tables, the following conclusions can be drawn:

- 1) **Table 7** and **Fig. 13** show that the DAG-MDAN still maintains its advantage in terms of accuracy performance. It is worth noting that in task $R_5, R_6, R_8 \rightarrow R_7$, S-DANN and M-DANN perform similarly, and even in task $R_5, R_7, R_8 \rightarrow R_6$, the accuracy of S-DANN is higher than M-DANN. This confirms the conclusion obtained in **Case I** that simply combining multiple source domains may lead to negative transfer and reduce the model performance. This also proves the importance of effective use of multi-source domain information as proposed in this paper.
- 2) **Fig. 14** shows that the accuracy of the DAG-MDAN fluctuates relatively smoothly over the ten experiments, indicating the robustness of the proposed method. **Fig. 12** shows that the proposed method is more capable of breaking the bottleneck in the training process. In addition, during the training process, we noticed that the CNN and MMD converge faster and the accuracy rate floats smoothly, which indicates that CNN and MMD have a more lightweight and stable structure, which is beneficial to the rapid convergence of the model. But when facing to complex cross-domain data distribution, they have a gap compared to the models with domain adaptation module.
- 3) As can be seen from **Fig. 15**, after removing the IA-Module ((i)-(o)), the target domain features will only overlap with at most one source domain feature, which is obviously not in line with the original intention of multi-domain adaptation. And in ((a)-(h)), the source-target domain features are better fused, and for each class of faults at least two domains cover the target domain, which proves the effectiveness of the dual adversarial module again.

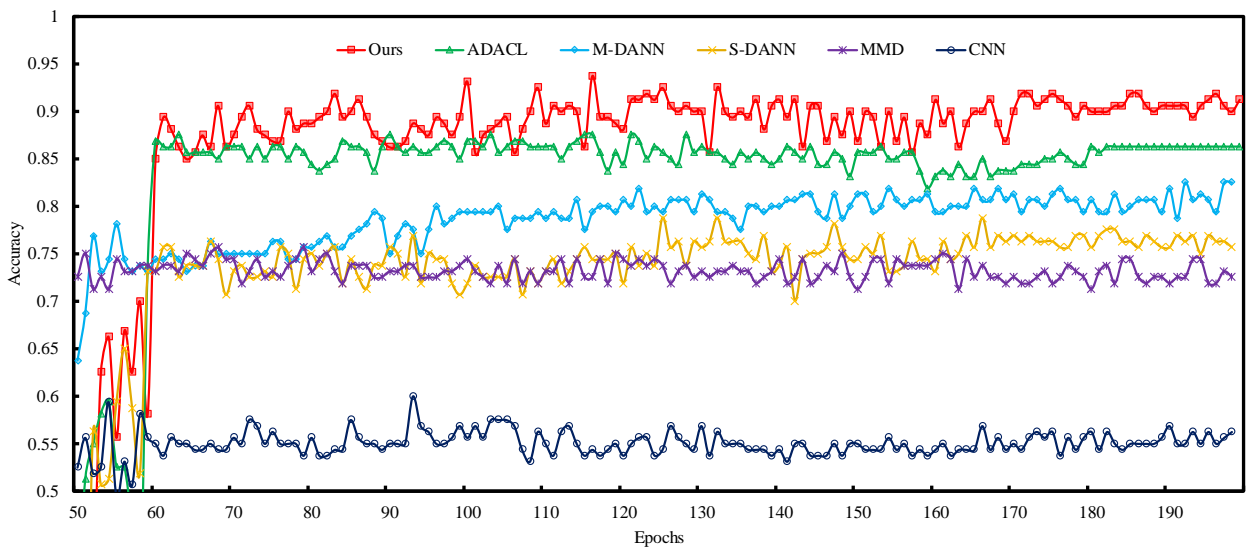


Fig. 12. Convergence of each method in the gearbox fault diagnosis transfer task $R_6, R_7, R_8 \rightarrow R_5$.

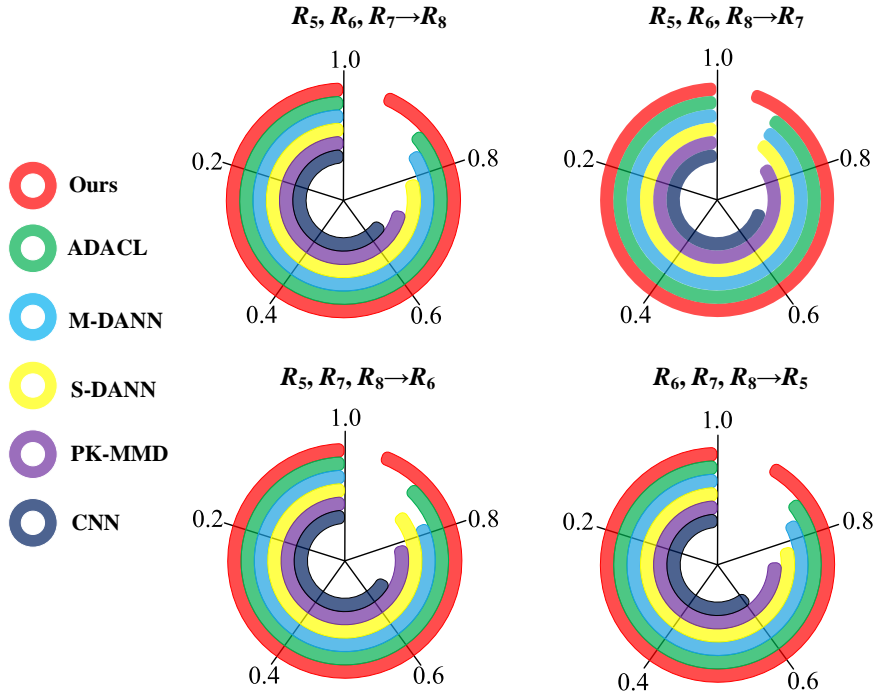


Fig. 13. Accuracy rings for each method in different gearbox fault diagnosis transfer tasks.

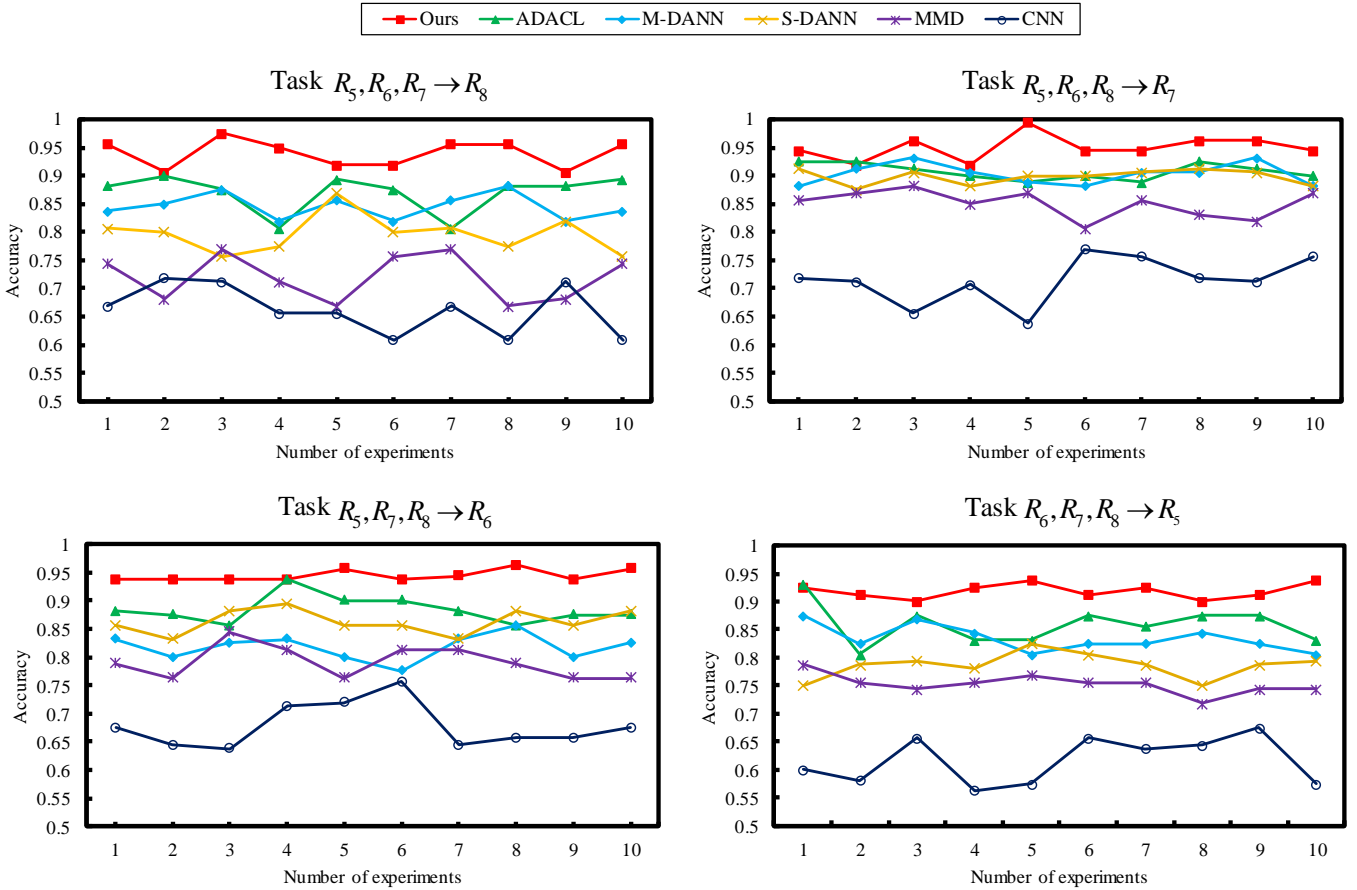


Fig. 14. Accuracy of 10 experiments with different methods in each gearbox fault diagnosis transfer task.

- 4) As can be seen from **Fig. 16**, embedding the MCD-Module maintains the accuracy advantage over removing the MCD-module, both in the early stage and late stage of training process, especially in the initial stage of training period, which can reduce the stumble of the model during the iterative process by the MCD-Module, speed up the model convergence, and help the model make better decisions when the model performs poorly.

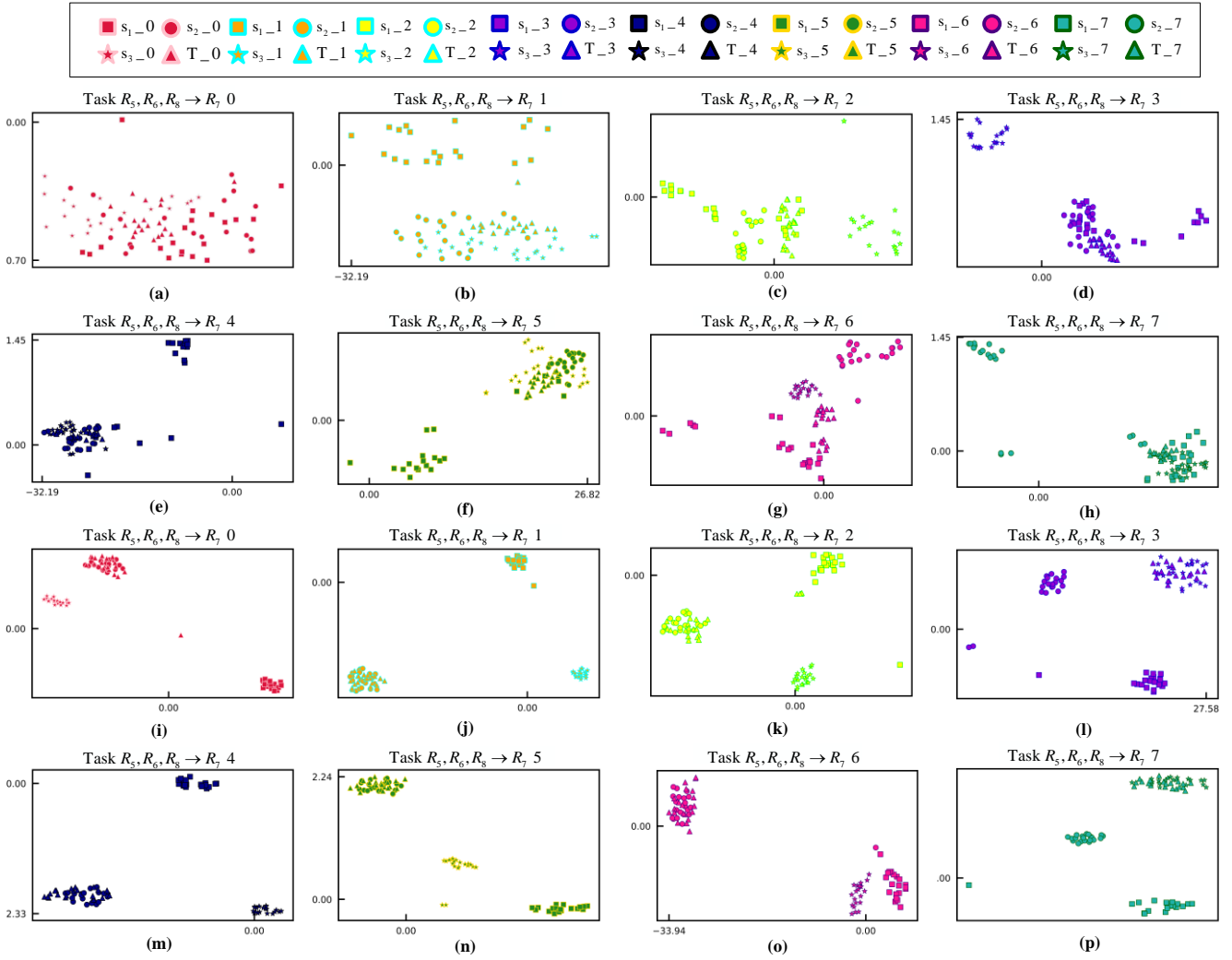


Fig. 15. Feature distribution under the gearbox fault diagnosis transfer task $R_5, R_6, R_8 \rightarrow R_7$: (a)(b)(c)(d)(e)(f)(g)(h) With IA-Module; (i)(g)(k)(l)(m)(n)(o)(p) Without IA-Module.

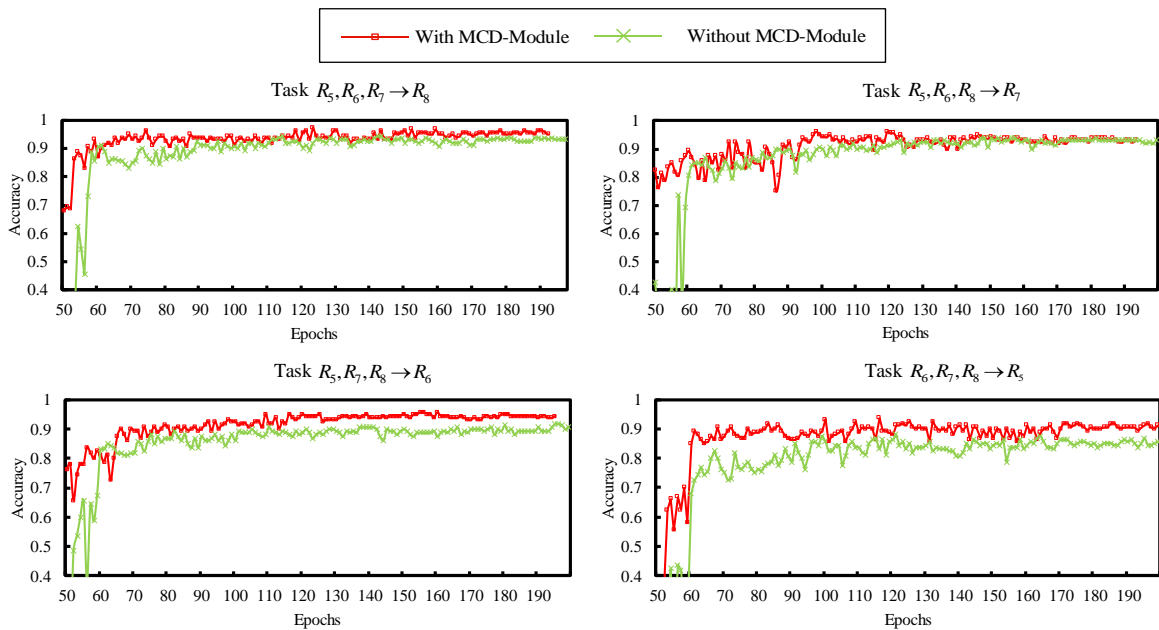


Fig. 16. Accuracy comparison between the training process of with MCD-Module and without MCD-Module.

5. Conclusion

For the unsupervised cross-domain fault diagnosis of rotating machine, the DAG-MDAN is proposed. By designing an inner adversarial module to fuse the multi-source-target domain feature, a multi-subnet collaborative decision module is proposed to make the final diagnosis results for the model. The proposed DAG-MDAN effectively utilizes multi-source domain diagnosis knowledge and improves the accuracy of rotating machine fault diagnosis.

Two multi-domain fault rotating machine datasets based on different rotational speed is used, and the results show the superiority and robustness of the DAG-MDAN compared with the comparison methods. Multi-source domain transfer learning is promising to effectively utilize source domain knowledge for fault diagnosis, but the multi-domain sample imbalance problem may significantly reduce the diagnosis performance, which will be the focus of future research.

Declaration of Competing Interest

The authors declare that they have no known competing financial interests or personal relationships that could have appeared to influence the work reported in this paper.

Acknowledgements

This research is supported by the National Natural Science Foundation of China (No. 52275104) and the Natural Science Fund for Excellent Young Scholars of Hunan Province (No. 2021JJ20017).

References

- [1] S. Yan, H. Shao, Y. Xiao, B. Liu, J. Wan, Hybrid robust convolutional autoencoder for unsupervised anomaly detection of machine tools under noises, *Robot Cim-int Manuf.* 79(2023) 102441.
- [2] Y. Xiao, H. Shao, Z. Min, H. Cao, X. Chen, Multiscale dilated convolutional subdomain adaptation network with attention for unsupervised fault diagnosis of rotating machinery cross operating conditions, *Meas.* 204(2022) 112146.
- [3] Y. Xiao, H. Shao, S. Han, Z. Huo, J. Wan, Novel joint transfer network for unsupervised bearing fault diagnosis from simulation domain to experimental domain, *IEEE ASME Trans Mechatron.* 27(2022) 5254-5263.
- [4] X. Wang, H. He, L. Li, A hierarchical deep domain adaptation approach for fault diagnosis of power plant thermal system. *IEEE Trans. Industr. Inform.* 15(2019) 5139-5148.
- [5] L. Wen, L. Gao, X. Li, A new deep transfer learning based on sparse auto-encoder for fault diagnosis, *IEEE T. Syst. Man. CY-S.* 49(2019) 136-144.
- [6] H. Shao, W Li, B Cai, J Wan, Y Xiao, S Yan. Dual-threshold attention-guided GAN and limited infrared thermal images for rotating machinery fault diagnosis under speed fluctuation, *IEEE Transactions on Industrial Informatics.* 2022, DOI 10.1109/TII.2022.3232766.
- [7] M Chen, H Shao, H Dou, W Li, B Liu. Data augmentation and intelligent fault diagnosis of planetary gearbox using ILoFGAN under extremely limited samples, *IEEE Transactions on Reliability,* 2022, DOI 10.1109/TR.2022.3215243.
- [8] M Xia, H Shao, D Williams, S Lu, L Shu, Clarence W. de Silva. Intelligent Fault Diagnosis of Machinery Using Digital Twin-assisted Deep Transfer Learning, *Reliability Engineering & System Safety.* 215(2021), 107938.
- [9] W. Wang, Y. Lei, T. Yan, Residual convolution long short-term memory network for machines remaining useful life prediction and uncertainty quantification, *Journal of Dynamics, Monitoring and Diagnostics.* 1(2022), 2-8.
- [10] T. Hahn, C. Mechefske, Self-supervised learning for tool wear monitoring with a disentangled-variational-autoencoder, *International Journal of Hydromechatronics.* 4(2021), 69-98.
- [11] Y. Lei, B. Yang, X. Jiang, F. Jia, N. Li, A.K. Nandi, Applications of machine learning to machine fault

- diagnosis: A review and roadmap, *Mech. Syst. Signal Process.* 138 (2020) 106587.
- [12] Y. Zhang, Z. Ren, K. Feng, K. Yu, M. Beer, Z. Liu, Universal source-free domain adaptation method for cross-domain fault diagnosis of machines, *Mech. Syst. Signal Process.* 191(2023) 110159.
- [13] G. Li, J. Hu, D. Shan, J. Ao, B. Huang, Z. Huang, A CNN model based on innovative expansion operation improving the fault diagnosis accuracy of drilling pump fluid end, *Mech. Syst. Signal Process.* 187(2023) 109974.
- [14] H. Wang, S. Chen, W. Zhai, Data-driven adaptive chirp mode decomposition with application to machine fault diagnosis under non-stationary conditions, *Mech. Syst. Signal Process.* 188(2023) 109997.
- [15] R. Yan, F. Shen, C. Sun, X. Chen, Knowledge transfer for rotary machine fault diagnosis, *IEEE Sens. J.* 20 (2020) 8374–8393.
- [16] Y. Zhu, F. Zhuang, D. Wang. Aligning domain specific distribution and classifier for cross-domain classification from multiple sources, *The Thirty-Third AAAI Conference on Artificial Intelligence*, 2019.
- [17] Y. Lei, B. Yang, Z. Du, N. Lv, Deep transfer diagnosis method for machinery in big data era (in Chinese). *Chin J Mech Eng*, 55(2019):1-8.
- [18] Y. Xu, X. Tang, G. Feng, et al. Orthogonal on-rotor sensing vibrations for condition monitoring of rotating machines. *Journal of Dynamics, Monitoring and Diagnostics*, 1(2022), 29-36.
- [19] F. Natalia, J. Sinha, Theoretical validation of earlier developed experimental rotor faults diagnosis model, *International Journal of Hydromechatronics*, 4(2021), 295-308.
- [20] Z. Zhao, Q. Zhang, X. Yu, C. Sun, Applications of unsupervised deep transfer learning to intelligent fault diagnosis: a survey and comparative study. *IEEE Trans Instrum. Meas.* 70(2021) 3525828.
- [21] X. Wang, C. Shen, M. Xia, D. Wang, J. Zhu, Z. Zhu, Multi-scale deep intra-class transfer learning for bearing fault diagnosis. *Reliab Eng Syst Safe*, 202(2020) 107050.
- [22] W. Li, R. Huang, J. Li, Y. Liao, Z. Chen, G. He, R. Yan, K. Gryllias, A perspective survey on deep transfer learning for fault diagnosis in industrial scenarios: Theories, applications and challenges, *Mech. Syst. Signal Process.* 167(2022) 108487.
- [23] Q. Qian, Y. Qin, J. Luo, Y. Wang, F. Wang, Deep discriminative transfer learning network for cross-machine fault diagnosis, *Mech. Syst. Signal Process.* 186(2023) 109884.
- [24] Z. Wang, W. Huang, Y. Chen, Y. Jiang, G. Peng, Multisource cross-domain fault diagnosis of rolling bearing based on subdomain adaptation network. *Meas. Sci. Technol.* 33(2022) 105109.
- [25] H. Zheng, R. Wang, Y. Yang, Y. Li, M. Xu, Intelligent fault identification based on multisource domain generalization towards actual diagnosis scenario. *IEEE Trans. Ind. Electron.* 67(2020) 1293-1304.
- [26] Y. Qin, Q. Yao, Y. Wang, Y. Mao, Parameter sharing adversarial domain adaptation networks for fault transfer diagnosis of planetary gearboxes, *Mech. Syst. Signal Process.* 160(2021) 107936.
- [27] B. Yang, Y. Lei, F. Jia, N. Li, Z. Du, A polynomial kernel induced distance metric to improve deep transfer learning for fault diagnosis of machines, *IEEE Trans. Ind. Electron.* 67(2020) 9747-9757.
- [28] Q. Qian, Y. Qin, Y. Wang, F. Liu, A new deep transfer learning network based on convolutional auto-encoder for mechanical fault diagnosis, *Meas.* 178(2021) 109352.
- [29] X. Li, W. Zhang, Q. Ding, A robust intelligent fault diagnosis method for rolling element bearings based on deep distance metric learning. *Neurocomputing*, 310(2018) 77-95.
- [30] L. Guo, Y. Lei, S. Xing, T. Yan, N. Li, Deep convolutional transfer learning network: a new method for intelligent fault diagnosis of machines with unlabeled data, *IEEE Trans Ind Electron*, 66(2019) 7316-7325.
- [31] B. Yang, Y. Lei, F. Jia, S. Xing, An intelligent fault diagnosis approach based on transfer learning from laboratory bearings to locomotive bearings, *Mech Syst Signal Pr*, 122(2019) 692-706.
- [32] X. Li, W. Zhang, Q. Ding, X. Li, Diagnosing rotating machines with weakly supervised data using deep transfer learning, *IEEE Trans Industr Inform*, 16(2020) 1688-1697.
- [33] J. Zhu, N. Chen, C. Shen, A new multiple source domain adaptation fault diagnosis method between different rotating machines, *IEEE Trans Industr Inform*, 17(2021) 4788-4797.
- [34] Y. Zhang, Z. Ren, S. Zhou, T. Yu, Adversarial domain adaptation with classifier alignment for cross-domain intelligent fault diagnosis of multiple source domains, *Meas Sci Technol*, 32(2021) 035102.

- [35] T. Han, Y. Li, M. Qian, A hybrid generalization network for intelligent fault diagnosis of rotating machinery under unseen working conditions, *IEEE Trans. Instrum. Meas.* 70(2021) 3520011.
- [36] C. Shen, Y. Xia, X. Jiang, Z. Chen, L. Kong, Z. Zhu, Optimal transport-based multisource student teacher learning network for bearing fault diagnosis under variable working conditions, *IEEE Sens. J.* 22(2022) 16392-16401.
- [37] X. Li, H. Jiang, M. Xie, T. Wang, R. Wang, Z. Wu, A reinforcement ensemble deep transfer learning network for rolling bearing fault diagnosis with Multi-source domains, *Adv. Eng. Inform.* 51(2022) 101480.
- [38] A. Gretton, K. Borgwardt, M. Rasch, B. Schoelkopf, A. Smola, A kernel two-sample test. *J Mach Learn Res*, 13(2012) 723-773.
- [39] W. Zellinger, T. Grubinger, E. Lughofer, T. Natschlger, S Saminger-Platz, Central moment discrepancy (CMD) for domain-invariant representation learning, *ICIR*, 2017
- [40] Y. Ganin, E. Ustinova, H. Ajakan, P. Germain, H. Larochelle, F. Laviolette, M. Marchand, V. Lempitsky, Domain-adversarial training of neural networks. *J Mach Learn Res*, 17(2016) 2096-2030.
- [41] H. Cao, H. Shao, X. Zhong, Q. Deng, X. Yang, J. Xuan, Unsupervised domain-share CNN for machine fault transfer diagnosis from steady speeds to time-varying speeds. *J Manuf Syst*, 62(2022) 186-198.
- [42] L. Maaten, G. Hinton, Visualizing data using t-SNE. *J Mach Learn Res*, 9(2008) 2579-2605.